PCCP

COMMUNICATION

View Article Online
View Journal | View Issue

High DNP efficiency of TEMPONE radicals in liquid toluene at low concentrations†

Cite this: *Phys. Chem. Chem. Phys.*, 2014, **16**, 8795

Received 27th February 2014,
Accepted 19th March 2014

DOI: 10.1039/c4cp00854e

www.rsc.org/pccp

Nikolay Enkin, Guoquan Liu,* Igor Tkach and Marina Bennati*

We show that at low concentrations (≤5 mM) TEMPONE radicals in liquid toluene exhibit higher DNP efficiency than in water. In spite of reduced coupling factors, the improved DNP performance in toluene results from favourable saturation and leakage factors, as determined by pulse electron–electron double resonance (ELDOR) and NMR relaxation, respectively. The extracted coupling factors at 0.35 Tesla support theoretical predictions of the Overhauser mechanism.

Dynamic nuclear polarization (DNP) is an emerging technique to enhance NMR signals and thus to improve the sensitivity or the contrast of NMR/MRI signals. In a DNP experiment, paramagnetic species, the so-called polarizers, transfer their spin polarization to hyperfine coupled nuclei when subjected to microwave irradiation. Over the last decade, the method has been extensively developed in different laboratories for NMR applications at high magnetic fields.[1–7]

In liquids, DNP is governed by the Overhauser mechanism,[8] in which the enhancement is proportional to the gyromagnetic ratios of the electron and the interacting nuclear spin (γ_e/γ_n), the coupling factor ξ, the leakage factor f and the saturation factor s:[9,10]

$$\varepsilon = 1 - s \cdot f \cdot \xi \cdot \frac{|\gamma_e|}{\gamma_I} \qquad (1)$$

The most important is the coupling factor, which depends on the intrinsic electron–nuclear spin relaxation and determines the efficiency of DNP under the most favourable conditions (*i.e.* $s = 1$ and $f = 1$). In the past few years, considerable attention has been devoted to the DNP mechanism of nitroxide radicals in water because of the excellent capabilities of these polarizers to adapt to biological environments for applications in biological systems.[11,12] For the nitroxide–water system, DNP efficiency is governed by dipolar relaxation and the maximum achievable enhancement is limited by $\xi_{max} = 0.5$, a factor which considerably decreases at higher magnetic fields.[13] This limit could be potentially overcome by taking advantage of other mechanisms, such as scalar relaxation contributions,[14] $\xi_{max} = -1$, or moreover starting from hyperpolarized electronic spin states.[15] To exploit these new avenues, some modifications in the polarizer–solvent system are required. Due to the difficulty in predicting coupling factors, which depend on the detailed atomistic interactions between the polarizer and the solvent as well as system-specific correlation functions of molecular motion, any chemical variations in the polarizer molecule or the solvent might lead to large changes in the DNP efficiency.

Recently, DNP with nitroxides in non-aqueous solvents, such as toluene[16,17] or benzene,[18] has been reconsidered by taking advantage of instrumental developments at different magnetic fields and progress in analysis. These non-polar solvents might be particularly attractive to host more complex organic polarizers and have the great advantage of low dielectric losses, which attenuate microwave heating. The latter facilitates mechanistic studies, which are critically dependent on temperature, and allows for the use of sample sizes close to standard NMR tubes. In the recent studies on nitroxides in toluene[17] and hexane,[18] large negative ^{1}H-NMR enhancements of the solvent on the order of or even higher than those in nitroxide–water have been observed. In the toluene study a different behavior of the ring and methyl ^{1}Hs was observed, however, a precise determination of coupling factors was hampered by the uncertainty about the saturation factor. Subsequently, a new theoretical approach was proposed to compute DNP coupling factors by combining MD simulations with analytical calculations of spectral densities at different magnetic fields.[19,20] Particularly, these studies provided predictions for the site-specific DNP enhancements of different toluene ^{1}Hs based on the molecular shape and dynamics. The same studies questioned the use of classical models[21] in liquid DNP to determine atomistic parameters, such as the distance of

Max-Planck Institute for Biophysical Chemistry, Am Fassberg, 37077 Göttingen, Germany. E-mail: guoquan.liu@mpibpc.mpg.de, marina.bennati@mpibpc.mpg.de

† Electronic supplementary information (ESI) available: The DNP setup, evaluation of enhancements, comparison of leakage factors in toluene and water, power and concentration dependence of the TEMPONE CW-EPR line in toluene, EPR and ELDOR recovery curves at 0.1 and 3 mM TEMPONE concentrations, an estimate of exchange coupling from the EPR line width. See DOI: 10.1039/c4cp00854e

the closest approach between the polarizer and the solvent. Nevertheless, experimental coupling factors are still missing in support of this study.

In this communication we present DNP experiments with ^{15}N- and ^{2}H-labelled TEMPONE (4-Oxo-TEMPO) in toluene solutions at 0.35 Tesla and an electron Larmor frequency of 9 GHz. This frequency is interesting for DNP in liquid state because of the large achievable enhancements and the possibility to combine it with high frequency NMR detection within a shuttle spectrometer.[22] We are able to distinguish two kinds of ^{1}H in toluene, *i.e.* the ring and the methyl ^{1}Hs. We find that DNP enhancements in toluene as compared to water are significantly larger in the low concentration regime ($\leq$5 mM) but reach similar maximum values at higher concentrations. The finding is investigated by electron–electron double resonance (ELDOR) and NMR to independently determine the saturation and the leakage factors.

In Fig. 1a we display representative room-temperature ^{1}H-14 MHz NMR spectra of degassed toluene doped with 5 mM TEMPONE-D-^{15}N. Two peaks can be resolved with a separation of about 70 Hz, corresponding to 5 ppm, which are consistent with the resonances of the ring and the methyl ^{1}H of toluene. After irradiation by microwave (mw), on-resonant with the radical EPR absorption (low-field hyperfine line), the NMR signal is enhanced by more than two orders of magnitude. We note that the polarizer concentration here is significantly lower than that usually reported in DNP experiments in liquids (20–100 mM). The DNP enhancements ε_{ring} and ε_{methyl} were determined to be −159 and −137 with an error of approx. ±5% from the first point of the free induction decay (ESI†). The enhancement does not further increase with the radical concentration (Fig. 1b). A comparison with the enhancement of water under similar conditions of mw irradiation ($B_1 \approx 3$ G) shows that DNP enhancements of toluene are substantially higher at low concentrations; however, they reach slightly lower maximum values ε_{max} at high concentrations.

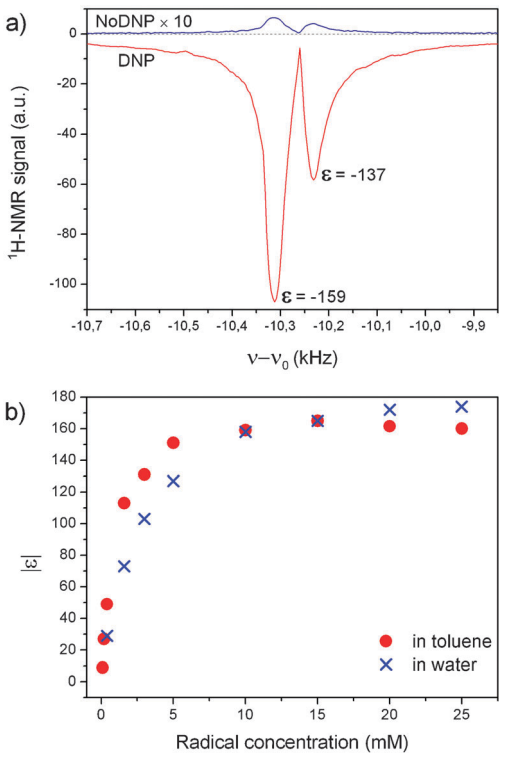

Fig. 1 (a) ^{1}H NMR spectra of toluene doped with 5 mM TEMPONE-D-^{15}N at 14 MHz. (b) Concentration dependence of DNP enhancements (from maximum of ε_{FID}) of TEMPONE-D-^{15}N in toluene and in water. Experimental details for toluene: samples degassed by three freeze–pump–thaw cycles, volumes of 20 μL, 1 or 8 scans for DNP measurements, 128 scans for Boltzmann measurements, $P_{mw} \approx 3$ W, $t_{irrad.}$ = 2–30 s depending on the concentration. For aqueous samples: non-degassed, V = 0.6 μL, 64 scans for DNP measurements and 1024 scans for Boltzmann measurements, t_{irrad} = 1–5 s. Details of the experimental set up are given in ref. 23 and in the ESI.†

Before analysing the observed enhancements, heating effects during mw irradiation need to be carefully examined. An increase in sample temperature leads to higher coupling factors and consequently higher enhancements.[24] According to previous DNP studies, heating effects were observed in water solutions at 9 GHz if the sample was exposed to the electric field of the microwaves.[23,25–27] Heating effects are usually manifested through lengthening of the build-up time of the DNP signal ($T_{buildup}$), which is otherwise determined by the relaxation rate of the detected nucleus in the presence of the polarizer (T_{1n}).[28] For all samples in this study, the filling height amounted to $\leq$5 mm, according to the homogeneity of the B_1 mw field in the dielectric resonator along the z-axis.[23] The inner diameter (ID) of the tube was optimized by measurements of the DNP build-up times and comparison with nuclear T_{1n}. For toluene sample tubes with an ID of 3 mm, $T_{buildup}$ for both ^{1}H types was found to be similar (within a 10% error limit) to T_{1n} measured independently from inversion recovery (Table 1).

From T_{1n} we could also evaluate the leakage factors f according to the definition:

$$f = \frac{R_{para} - R_{dia}}{R_{para}} = 1 - \frac{R_{dia}}{R_{para}} \qquad (2)$$

where $R_{para} = \frac{1}{T_{1n}}$ and $R_{dia} = \frac{1}{T_{dia}}$ are the spin–lattice relaxation rates of the toluene ^{1}Hs in the presence and absence of the radical, respectively.[24] The diamagnetic contribution amounted to 0.06 s^{-1} for the ring and 0.1 s^{-1} for the methyl protons, in agreement with the values reported in ref. 17. The leakage factors from eqn (2) are listed in Table 1. The ring protons exhibit slightly larger leakage factors f compared to the methyl protons at all concentrations, which is consistent with previous results obtained at 3.4 Tesla.[17] A comparison with the leakage factors in water indicates that the larger R_{dia} of water (0.33 s^{-1}) is responsible for reducing f in water as compared to toluene (Fig. S1, ESI†).

The concentration dependence of the DNP enhancements of TEMPONE-D-^{15}N in toluene (Fig. 1b) suggests similar coupling factors as in water but a peculiar behaviour of the saturation factor. To clarify this point, pulsed ELDOR was applied to directly measure the effective saturation of both nitroxide lines

Table 1 Summary of DNP parameters for toluene doped with TEMPONE-D-^{15}N

	ε		$T_{buildup}$ (s)		T_{1n} (s)		f					ξ	
Concentration (mM)	H_{ring}	H_m	H_{ring}	H_m	H_{ring}	H_m	H_{ring}	H_m	T_{2e}[b] (ns)	$s_{2,max}$	s_{eff}	H_{ring}	H_m
0.2	32	18	12.1	8.9	10.7	7.4	0.34	0.24	171	0.18	0.59	0.25	0.21
0.4	58	34	8.0	6.4	—	—	0.51[a]	0.34[a]	152	0.34	0.67	0.26	0.23
1.6	124	94	3.3	3.1	3.2	3.2	0.80	0.67	98	0.66	0.83	0.28	0.26
5.0	159	137	1.2	1.3	1.4	1.6	0.91	0.84	48	0.84	0.92	0.29	0.26

[a] Calculated from $T_{buildup}$. [b] From EPR line width, Fig. S3 (ESI).

s_{eff} when only one EPR line was excited by microwaves.[29] Preconditions for this dual frequency experiment are the detection of the radical FID as well as the capability to pump and detect both EPR lines within the EPR resonator. For a separation of ~60 MHz of the ^{15}N nitroxide hyperfine lines (Fig. S3, ESI†), the experiment is well feasible at 9 GHz within the band width of a standard overcoupled dielectric resonator. On the other hand, the detection of an EPR-FID depends on T_2, which usually shortens at higher concentrations due to concentration dependent relaxation contributions (exchange and dipolar couplings). For TEMPONE in toluene, detection of the FID was possible only at concentrations up to about 5 mM.

The EPR-FID intensity as a function of the frequency of the saturation pulse is depicted in Fig. 2. When the saturation pulse was resonant with the detection frequency, a complete drop in the FID signal was achieved at all concentrations (up to 5 mM). This corresponds to a full saturation ($s_1 = 1$) of the excited EPR line. A second drop in FID was visible when the saturation pulse became resonant with the second hyperfine transition. This reduction in FID directly corresponds to the saturation factor of the coupled hyperfine line (s_2).[29–31] The effective saturation factor s_{eff} of the total EPR spectrum is then the average of s_1 and s_2, *i.e.* $s_{eff} = (s_1 + s_2)/2$. To correlate s_2 and s_{eff} as determined by ELDOR with s_{eff} of DNP in eqn (1), one should perform both experiments at comparable microwave excitation fields. On the other hand, the saturation factor of the coupled hyperfine line reaches a maximum value $s_{2,max}$, when the excited line is saturated ($s_1 = 1$).[29] The condition $s_1 = 1$, which is well satisfied in the ELDOR experiment (Fig. 2), was tested in the DNP setup by recording the intensity of the excited EPR transition as a function of the microwave power (Fig. S2, ESI†). For $P \sim 3$ W, saturation s_1 close to unity was achieved at the investigated concentrations. Therefore, the saturation factors from Fig. 2a can be used to calculate $s_{eff,max}$ for DNP (Table 1). Fig. 2b illustrates a comparison of $s_{2,max}$ of TEMPONE-D-^{15}N in toluene and in water (data for water from ref. 29). The former increases rapidly with the radical concentration and it is larger than that in water at comparable concentrations.

Saturation factors $s_{eff,max} > 0.5$ of TEMPONE in water have been previously attributed to the effect of Heisenberg exchange between the spin states of the two hyperfine lines according to:[29]

$$s_{2,max} = 1 - \frac{2}{\left(2 + \frac{w_n}{w_e} + \frac{\omega_{ex}}{2w_e}\right)} \quad (3)$$

where ω_{ex} is the Heisenberg exchange rate, and w_n and w_e are the transition rates for the intramolecular electron and nuclear (^{15}N) spin relaxation, respectively. w_n and w_e are not concentration dependent‡ and cannot account for the behaviour observed in Fig. 2b. Nevertheless, ω_{ex} cannot be extracted from eqn (3) independently from T_{1e}. To examine ω_{ex}, we measured the polarization recovery of the hyperfine lines using detection and pumping pulses at the same frequency or at two EPR frequencies (*i.e.* pumping one hyperfine line and observing the second line). Following our previous treatment[29] the time evolution of the FID

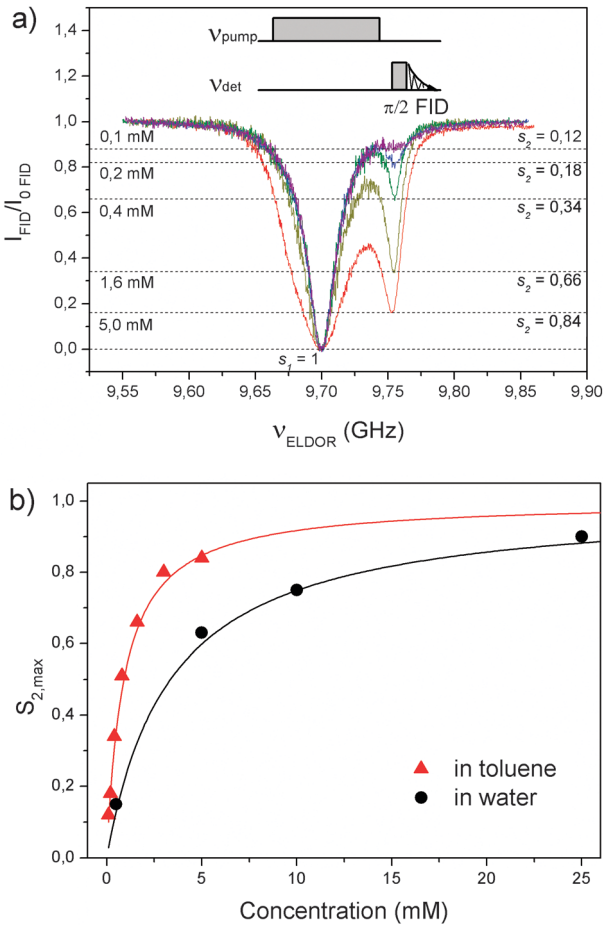

Fig. 2 (a) EPR-FID intensity of the high-field hf line of TEMPONE-D-^{15}N as a function of the frequency of the saturating (pump) pulse. Exp. details: detection is 30 MHz off resonance on the high field side to minimize simultaneous excitation of the low field line; t (π/2) = 16 ns; t (pump) = 1 μs. B_1 ~2–3 G. Error due to ringing was ≤10%. (b) Concentration dependence of $s_{2,max}$. Saturation data for water are from ref. 29. Red and black traces are calculated according to eqn (3) for toluene and water samples, respectively. T_{1e} for water is 298 ns.[29]

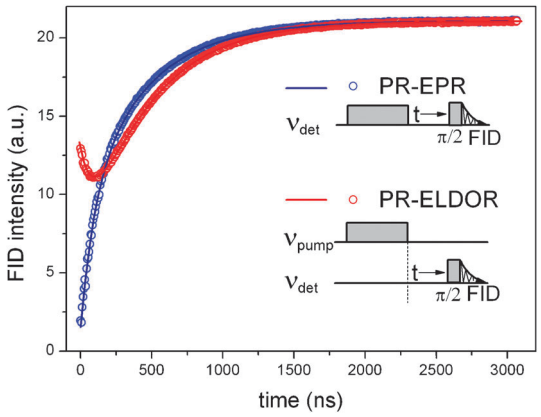

Fig. 3 Recovery curves and fits of the FID in EPR and ELDOR polarization recovery measurements at 1.6 mM TEMPONE-D-^{15}N in toluene. Experimental setup and conditions are similar to those given in Fig. 2.

signals for hyperfine lines 1 and 2 (i_1 and i_2) after a saturating pulse is described by:

$$i_{1,2} = A_{1,2}e^{-2w_e t} \pm B_{1,2}e^{-(2w_e + 2w_n + \omega_{ex})t} \quad (4)$$

where the amplitudes $A_{1,2}$ and $B_{1,2}$ are given by the initial FID intensities. The data were recorded using the same setup as that used for the ELDOR experiment in Fig. 2 but by varying the time delay between saturating and detection pulses (Fig. 3, inset). Fig. 3 illustrates the recovery curves for TEMPONE-D-^{15}N in toluene at a concentration of 1.6 mM. The polarization recovery of the coupled hyperfine line (red curve) shows the intrinsic counteracting mechanism of polarization decay (ELDOR effect) and recovery by T_{1e}. By assuming $w_n \ll w_e$ and fitting both curves with a shared set of exponentials, we obtained T_{1e} of 442 ± 50 ns and an exchange coupling rate ω_{ex} = (8 ± 1) × 10^6 s^{-1}. To test whether ω_{ex} accounts for the concentration dependence of $s_{2,max}$, we simulated the latter behaviour using eqn (3) and assuming $\omega_{ex} = n{\cdot}K_x$§ where n is the radical concentration and K_x is the normalized rate per mole.[32] As shown in Fig. 2b, a value of K_x = (5.0 ± 0.7) × 10^9 s^{-1} M^{-1} reproduces $s_{2,max}$ in the investigated concentration range satisfactorily. We noted that this value of K_x is higher than the counterpart of TEMPONE-D-^{15}N in water (K_x of 2.0 × 10^9 s^{-1} M^{-1}) by a factor of 2.5.[29] Heisenberg exchange has been previously treated as a bimolecular interaction with a rate proportional to the translational diffusion coefficient: $\omega_{ex} \sim D$.[30,33] For Brownian motion in liquids, the latter is in turn inversely proportional to the viscosity η through the Stokes–Einstein relation: $D \sim 1/\eta$. In the strong exchange limit[30,33] the coupling constant reduces to $K_x = \omega_{ex}/n = 8kT/3\eta$. An estimate for toluene within this limit leads to K_x = 1.1 × 10^{10} s^{-1} M^{-1}. The value exceeds the experimental one by a factor of 2, which in turn seems to be consistent with the trend reported in ref. 30 when comparing theory with experiment. As compared to water, at room temperature (20 °C) the viscosities are 1.0 mPa s and 0.590 mPa s for water and toluene, respectively. Clearly, the difference in viscosities accounts only partially for the difference in exchange coupling rates and accordingly the saturation factors. The exchange in water, which is weaker than in toluene, is likely not well reproduced by the classical model of strong exchange coupling. This is somehow not surprising given the different electronic structures of the two solvents, specifically the delocalized electronic system in toluene. Recent quantum chemical calculations pointed out the role of electron delocalization effects in through-bond and through-space electron–electron interactions.[34] Values of the exchange constants similar to that of the TEMPONE–toluene system were reported for TEMPO in benzene and di-fluorobenzene.[18]

With the availability of all factors in eqn (1) except ξ, we were then able to determine the coupling factors for the ring and methyl ^{1}H of toluene doped with TEMPONE at 0.35 T. This value was calculated at each concentration and is listed in Table 1. As expected, ξ is independent of the radical concentration within the error limit and averages to 0.27 and 0.24 for the ring and the methyl ^{1}Hs, respectively.¶ The error is estimated to be ±0.025 (about 10%) and is larger at lower concentrations due to the weaker S/N ratio. However, the error in trend (difference between the average ξ of the two ^{1}H types) is much less, as seen from the data in Table 1. Therefore the difference between the ξs is significant.

The magnitude of ξ for the ^{1}Hs of toluene is less than that of the water protons (ξ_{water} = 0.33[29]) using the same radical polarizer. One might not exclude *a priori* that the observed ξ results from counteracting scalar and dipolar relaxation mechanisms, although the dipolar mechanism is reportedly dominant for ^{1}H. If pure dipolar relaxation is dominated by a single correlation function, the coupling factor can be estimated from the nuclear relaxation rates:[9]

$$\xi \approx \frac{5}{7}\left\{1 - \frac{2w_I}{R_I - R_I^0}\right\} \quad (5)$$

where R_I^0 is the nuclear relaxation rate without a paramagnet, R_I and $2w_I$ are the relaxation rates at the observing field and the high field limit, respectively. Inserting for the ring protons R_I^0 = 0.06 s^{-1}, R_I (at 5 mM) = 0.714 s^{-1} (Table 1) and $2w_I$ (at 5 mM, 300 MHz ^{1}H NMR) ≈ 0.42 s^{-1} from ref. 17 we arrive at $\xi \approx 0.25$ (within 10–15% error limit), which is very close to the experimental value. Therefore, the reduction of the coupling factor of the toluene protons is consistent with a DNP mechanism dominated by dipolar relaxation. A more precise interpretation of relaxation contributions requires NMRD (relaxation dispersion) analysis.

Our results reveal a difference in the coupling factors between the ring and methyl protons that has not been inferred to date experimentally due to the lack of information about the saturation behaviour. In a previous 94 GHz/3 T study on TEMPOL/toluene,[17] larger DNP enhancements of the ring protons were observed but attributed to a favourable leakage factor. The present results are mechanistically significant as the obtained coupling factors are in excellent agreement with recent theoretical predictions[19] (ξ_{ring}^{theor} = 0.268; ξ_{methyl}^{theor} = 0.25 at 9.6 GHz mw frequency) performed using a sophisticated combination of MD simulations and analytical expressions of spectral densities for dipolar relaxation in the TEMPOL/toluene system.

The MD trajectories allowed to capture the dynamics of the polarizer and the solvent within the short interaction range (<1 nm) and to extract appropriate dipolar correlation functions. The larger ξ^{theor} of the ring protons was found to be associated to a larger radial density distribution at the closest possible distance to the electron spin of the nitroxide group. The agreement between our experiment and theory at this level of atomistic details is encouraging and opens up new prospects for the application of DNP to investigate molecular dynamics.

Conclusions

DNP experiments with TEMPONE in toluene at 0.35 T revealed that large signal enhancements ($\varepsilon \geq 100$) could be achieved at low polarizer concentrations ($c \leq 5$ mM), which makes this solvent attractive for future developments and applications of DNP. The high DNP performance was rationalized by investigating the different parameters of the Overhauser equation. Most importantly, the saturation behaviour of the EPR line in toluene turned out to be very efficient due to a Heisenberg exchange coupling rate that is larger than that in water by a factor of ≥ 2. Knowledge of the saturation factor permitted us to evaluate the DNP coupling factors for the different protons of toluene that provide insight into the DNP mechanism at the atomistic level. Our results support a recent theoretical MD investigation, by which the coupling factors in toluene reflect the detailed motion of the solvent protons around the atoms bearing the electron spin.

Acknowledgements

We would like to thank Giacomo Parigi and Deniz Sezer for discussion. We acknowledge financial support from the Max Planck Society and the COST Action TD1103 (European Network on Hyperpolarization). NE acknowledges the Graduate School for Neurosciences, Biophysics and Molecular Biosciences in Göttingen (GGNB) for financial support.

Notes and references

‡ T_{1e} was also measured at 0.1 and 3 mM TEMPONE concentrations, as displayed in Fig. S4 (ESI†). Values were found to be distributed within the error limit given in the text, likely due to the slightly different oxygen content.
§ This is not always valid and has to be verified from case to case. A comparative estimate of ω_{ex} obtained from the EPR line broadening is reported in Fig. S5 (ESI†). The value of $K_x = (4.3 \pm 0.5) \times 10^9\ s^{-1}\ M^{-1}$ is within the error limit as given in the text. However, determination from line broadening seems to be less accurate.
¶ The coupling factor at low concentrations is likely to be underestimated due to insufficient irradiation time. We did not use longer irradiation times to avoid heating in the resonator and in the sample.

1 T. Maly, G. T. Debelouchina, V. S. Bajaj, K. N. Hu, C. G. Joo, M. L. Mak-Jurkauskas, J. R. Sirigiri, P. C. A. van der Wel, J. Herzfeld, R. J. Temkin and R. G. Griffin, *J. Chem. Phys.*, 2008, **128**, 052211.
2 J. H. Ardenkjaer-Larsen, B. Fridlund, A. Gram, G. Hansson, L. Hansson, M. H. Lerche, R. Servin, M. Thaning and K. Golman, *Proc. Natl. Acad. Sci. U. S. A.*, 2003, **100**, 10158–10163.
3 P. Höfer, G. Parigi, C. Luchinat, P. Carl, G. Guthausen, M. Reese, T. Carlomagno, C. Griesinger and M. Bennati, *J. Am. Chem. Soc.*, 2008, **130**, 3254–3255.
4 R. G. Griffin and T. F. Prisner, *Phys. Chem. Chem. Phys.*, 2010, **12**, 5737–5740.
5 J. G. Krummenacker, V. P. Denysenkov, M. Terekhov, L. M. Schreiber and T. F. Prisner, *J. Magn. Reson.*, 2012, **215**, 94–99.
6 C. Y. Cheng and S. I. Han, *Annu. Rev. Phys. Chem.*, 2013, **64**, 507–532.
7 Q. Z. Ni, E. Daviso, T. V. Chan, E. Markhasin, J. Sudheer, T. M. Swager, R. J. Temkin, J. Herzfeld and R. G. Griffin, *Acc. Chem. Res.*, 2013, **46**, 1933–1941.
8 A. W. Overhauser, *Phys. Rev.*, 1953, **92**, 411–415.
9 D. Hausser and D. Stehlik, *Adv. Magn. Reson.*, 1968, **3**, 79–139.
10 W. Müller-Warmuth and K. Meise-Gresch, *Adv. Magn. Reson.*, 1983, **11**, 1–45.
11 M. Bennati, I. Tkach and M. T. Türke, in *Electron paramagnetic resonance*, ed. B. Gilbert, Royal Society of Chemistry, Cambridge, 2011, pp. 155–182.
12 M. D. Lingwood and S. Han, *Annu. Rep. NMR Spectrosc.*, 2011, **73**, 83–126.
13 C. Griesinger, M. Bennati, H. M. Vieth, C. Luchinat, G. Parigi, P. Höfer, F. Engelke, S. J. Glaser, V. Denysenkov and T. F. Prisner, *Prog. Nucl. Magn. Reson. Spectrosc.*, 2012, **64**, 4–28.
14 N. M. Loening, M. Rosay, V. Weis and R. G. Griffin, *J. Am. Chem. Soc.*, 2002, **124**, 8808–8809.
15 K. Tateishi, M. Negoro, A. Kagawa and M. Kitagawa, *Angew. Chem., Int. Ed.*, 2013, **52**, 13307–13310.
16 G. J. Krüger, W. Müller-Warmuth and R. Van Steenwinkel, *Z. Naturforsch., A: Astrophys. Phys. Phys. Chem.*, 1966, **21**, 1224–1230.
17 E. V. Kryukov, M. E. Newton, K. J. Pike, D. R. Bolton, R. M. Kowalczyk, A. P. Howes, M. E. Smith and R. Dupree, *Phys. Chem. Chem. Phys.*, 2010, **12**, 5757–5765.
18 O. Neudert, C. Mattea, H. W. Spiess, S. Stapf and K. Muennemann, *Phys. Chem. Chem. Phys.*, 2013, **15**, 20717–20726.
19 D. Sezer, *Phys. Chem. Chem. Phys.*, 2013, **15**, 526–540.
20 D. Sezer, *Phys. Chem. Chem. Phys.*, 2014, **16**, 1022–1032.
21 L. P. Hwang and J. H. Freed, *J. Chem. Phys.*, 1975, **63**, 4017–4025.
22 A. Krahn, P. Lottmann, T. Marquardsen, A. Tavernier, M. T. Turke, M. Reese, A. Leonov, M. Bennati, P. Höfer, F. Engelke and C. Griesinger, *Phys. Chem. Chem. Phys.*, 2010, **12**, 5830–5840.
23 M. T. Türke, I. Tkach, M. Reese, P. Höfer and M. Bennati, *Phys. Chem. Chem. Phys.*, 2010, **12**, 5893–5901.
24 M. Bennati, C. Luchinat, G. Parigi and M.-T. Türke, *Phys. Chem. Chem. Phys.*, 2010, **12**, 5902–5910.
25 M. Gafurov, V. Denysenkov, M. J. Prandolini and T. F. Prisner, *Appl. Magn. Reson.*, 2012, **43**, 119–128.
26 P. Neugebauer, J. G. Krummenacker, V. P. Denysenkov, G. Parigi, C. Luchinat and T. F. Prisner, *Phys. Chem. Chem. Phys.*, 2013, **15**, 6049–6056.

27 J. M. Franck, A. Pavlova, J. A. Scott and S. Han, *Prog. Nucl. Magn. Reson. Spectrosc.*, 2013, **74**, 33–56.
28 M. T. Türke and M. Bennati, *Appl. Magn. Reson.*, 2012, **43**, 129–138.
29 M. T. Türke and M. Bennati, *Phys. Chem. Chem. Phys.*, 2011, **13**, 3630–3633.
30 J. S. Hyde, J. C. W. Chen and J. H. Freed, *J. Chem. Phys.*, 1968, **48**, 4211–4226.
31 M. T. Türke, G. Parigi, C. Luchinat and M. Bennati, *Phys. Chem. Chem. Phys.*, 2012, **14**, 502–510.
32 B. L. Bales and M. Peric, *J. Phys. Chem. B*, 1997, **101**, 8707–8716.
33 J. D. Currin, *Phys. Rev.*, 1962, **126**, 1995.
34 C. Riplinger, J. P. Y. Kao, G. M. Rosen, V. Kathirvelu, G. R. Eaton, S. S. Eaton, A. Kutateladze and F. Neese, *J. Am. Chem. Soc.*, 2009, **131**, 10092–10106.